

Metal–antiferromagnetic-insulator transition in V_2O_3 alloys

S. A. Shivashankar* and J. M. Honig

Department of Chemistry, Purdue University, West Lafayette, Indiana 47907

(Received 20 January 1983; revised manuscript received 20 June 1983)

Electrical resistivity measurements are reported for a variety of $(V_{1-x}Ti_x)_2O_3$ and $V_{2(1-y)}O_3$ systems, with $0 \leq x < 0.06$ and $0 \leq y < 0.01$, in the range 20–300 K. The metal–antiferromagnetic-insulator transition temperature T_N diminishes steadily with increasing x and y and drops abruptly to zero at a critical concentration. The size of the discontinuity in electrical resistivity at T_N diminishes with T_N for the Ti-alloy system; for nonstoichiometric V_2O_3 it passes through a minimum and then rises significantly. These features can be rationalized almost quantitatively by assuming that acoustic lattice and ionized-impurity scattering processes govern the mobility of the itinerant charge carriers in the $(V_{1-x}Ti_x)_2O_3$ and $V_{2(1-y)}O_3$ systems, respectively.

I. INTRODUCTORY COMMENTS

The V_2O_3 system has been the subject of many investigations because it exhibits one or more sets of spectacular metal-insulator transitions which can be induced by changes in temperature or pressure, or by alloying. Of special relevance to the present investigation is the low-temperature transition in which the material undergoes a paramagnetic metal (PM) to antiferromagnetic insulator (AFI) transition upon cooling. It has been known for some time that this particular phase change may be drastically affected through addition of Ti_2O_3 ,^{1–18} or by rendering the material nonstoichiometric.^{19–37} Much of the earlier effort has centered on the study of magnetic or of crystallographic properties; investigations on electrical characteristics are largely contradictory and have frequently been carried out on sintered material which is inherently unsuited for quantitative investigations. Electrical measurements reported for single crystals of $(V_{1-x}Ti_x)_2O_3$ (Refs. 1, 4, 6, 9–11, 16, and 17) or of $V_{2(1-y)}O_3$ (Refs. 21–23, 25, 26, 28, 33, 36, and 37) are sporadic and/or were hampered by problems of preserving the crystals through the PM-AFI transition. Furthermore, no attempt has so far been made to analyze the features of the PM-AFI transition in quantitative detail. Thus it appeared appropriate to initiate a systematic investigation of the electrical properties of $(V_{1-x}Ti_x)_2O_3$ for $0 \leq x < 0.06$ and $V_{2(1-y)}O_3$ for $0 \leq y < 0.01$ on well-annealed single-crystal specimens, and to follow these measurements with a quantitative evaluation of the data.

II. EXPERIMENTAL WORK

Single crystals of Ti-doped V_2O_3 were grown from the melt by the Reed Tri-arc technique³⁸; nonstoichiometric single crystals were grown using a skull melter whose operation is described elsewhere.^{39,40} In both cases thin specimens were cut to the desired shape and then annealed in a suitable CO-CO₂ atmosphere for control of stoichiometry, as detailed by Shivashankar *et al.*⁴¹

Four-probe electrical resistivity measurements were carried out using a dip-tube cryostat equipped with a rapid-

feedback temperature regulator based on the use of an unencapsulated light-emitting diode⁴² (LED) for precise temperature control. Either a digital voltmeter or an electrometer was used to cope with the high impedances of the insulating phases. Current was periodically reversed to permit averaging out of spurious thermoelectric signals. In several cases an ac technique operating at 100 Hz was employed in conjunction with a lock-in amplifier.

III. RESULTS

The variation of electrical resistivity with temperature for $T < 300$ K is shown in Fig. 1 for Ti-doped specimens and in Fig. 2 for nonstoichiometric samples. One should note the following. (i) That the Néel temperature T_N of the PM-AFI transition drops markedly with increasing Ti content or with increasing deviation from stoichiometry. (ii) That the resistivity activation energy ϵ_σ diminishes rapidly with increasing Ti or O doping levels; as $\epsilon_\sigma \rightarrow 0$,

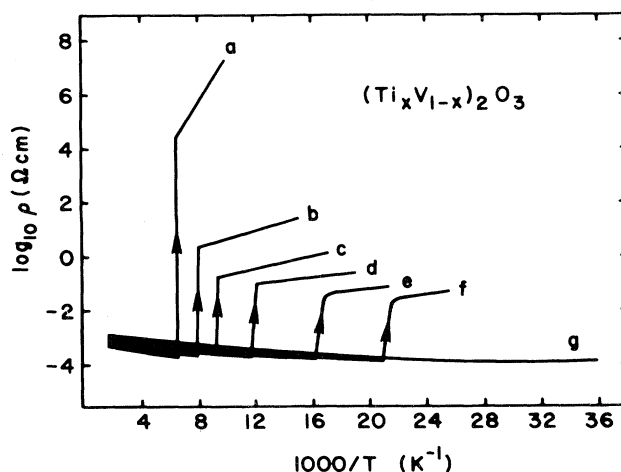


FIG. 1. Variation of electrical resistivity with temperature for $(V_{1-x}Ti_x)_2O_3$ alloys. Note reduction of size in resistivity discontinuity with the transition temperature T_N . The x values are a, 0.0; b, 0.01; c, 0.02; d, 0.03; e, 0.04; f, 0.049; and g, 0.055.

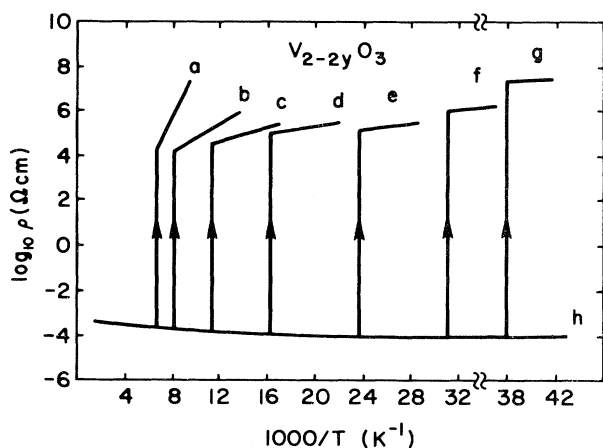


FIG. 2. Variation of electrical resistivity with temperature for $V_{2(1-y)}O_3$ (nonstoichiometric V_2O_3). Note the minimum in the size of the discontinuity of resistivity at the transition temperature $T_N \approx 110$ K. The y values are a, 0.0; b, 0.0045; c, 0.0055; d, 0.0065; e, 0.0072; f, 0.0075; g, 0.0075 +; and h, 0.0095 +.

the transition is eliminated altogether. (iii) The resistivity of all specimens in the metallic phase is very nearly independent of x or y and only weakly temperature dependent. Thus the resistivity jump for both the $(V_{1-x}Ti_x)_2O_3$ and $V_{2(1-y)}O_3$ systems is due almost entirely to changes in resistivity in the AFI phases. What distinguishes the Ti-alloy system from the cation-deficient specimens is (iv) the size of the electrical discontinuity $\Delta\rho$ which decreases significantly with T_N in the former case; it passes through a minimum and increases with diminishing T_N in the latter case.

The variations in the physical parameters T_N , ϵ_σ , and $\Delta \log_{10}\rho$ with x and with y are exhibited in Figs. 3 and 4,

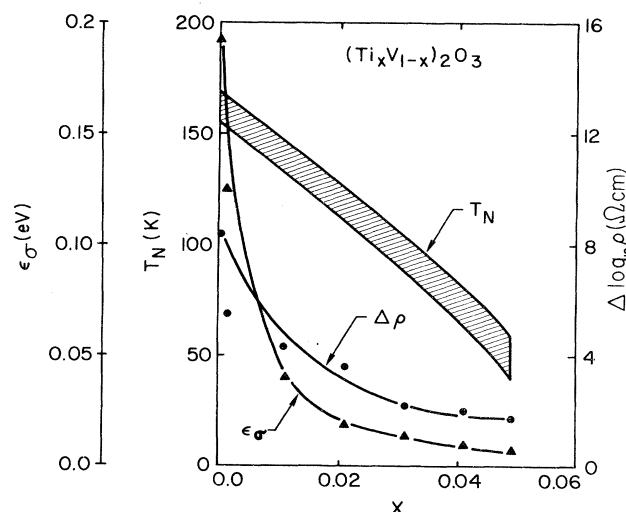


FIG. 3. Variation of transition temperature T_N , conductivity activation energy ϵ_σ , and logarithmic discontinuity in electrical resistivity $\Delta \log_{10}\rho$ with x for $(V_{1-x}Ti_x)_2O_3$ alloys. Shaded portion indicates size of hysteresis loop.

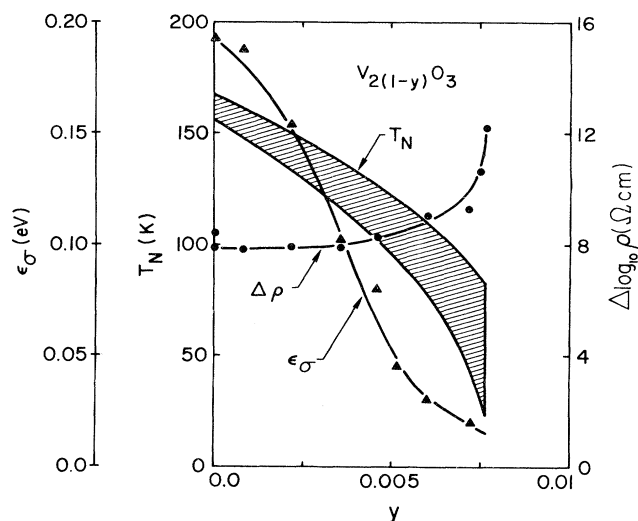


FIG. 4. Variation of transition temperature T_N , conductivity activation energy ϵ_σ , and logarithmic discontinuity in electrical resistivity $\Delta \log_{10}\rho$ with y for $V_{2(1-y)}O_3$. Shaded portion indicates size of hysteresis loop.

respectively. These results are in reasonable agreement with those assembled in Ref. 37(a). Examination of the two figures brings out additional points. (v) The transition terminates at a much higher critical density of Ti substitutions ($x_c \approx 0.05$) than it does for the case of vacancy concentrations ($y_c \approx 0.0085$). (vi) The hysteresis loop shown by the shaded regions in Figs. 3 and 4 is nearly independent of x ($\Delta T \approx 13$ K) but increases greatly (from $\Delta T \approx 13$ to 46 K) with y . This widening of the temperature hysteresis due to increasing nonstoichiometry is in accordance with the prediction made by Adler *et al.*^{37(b)} However, the reduction in the PM-AFI transition temperature due to nonstoichiometry is much larger than that predicted by these authors.

Our resistivity measurements for $(V_{1-x}Ti_x)_2O_3$ as summarized in Fig. 1 are in reasonable agreement with earlier measurements at other laboratories,^{1,4,9} and coincide very well with prior work at Purdue University.^{7,8,10} The above measurements seem to rule out one isolated report¹¹ according to which T_N remains unaffected by incorporation of Ti into the V_2O_3 host lattice. It is more difficult to compare present findings on $V_{2(1-y)}O_3$ with earlier work because the only really systematic studies were carried out on sintered specimens. With one exception,²² there is agreement at a qualitative level concerning the effects of changing stoichiometry on T_N , ϵ_σ , and $\Delta \log_{10}\rho$,^{21,23,25,26,34,37} but considerable differences remain at the quantitative level, perhaps because of absence of control over annealing procedures in the earlier investigations.

Earlier experiments on samples of low quality⁴³ have shown that some irreproducibility in the measurements is encountered on repeated cycling through the PM-AFI transition, due to the fact that cracks and fissures occasionally develop in the specimens, as a concomitant to the 1.5% change in unit-cell volume at the transformation. Often, the transition is accompanied by microcrack-

ing, which is minimized in thin specimens (200–300 μm) with small volume. However, none of these effects significantly altered the general trends exhibited in Figs. 1 and 2, and the transition temperatures always remained unaffected in the cycling processes.

As has recently been demonstrated by electron microscopy,⁴⁴ even at the extreme end of the homogeneous stoichiometry range of $\text{V}_{2(1-y)}\text{O}_3$ where $y \approx 0.009$, the degree of vacancy clustering is not appreciable. Thus it appears safe to conclude that the change in the PM-AFI transition temperature is a characteristic of the relatively homogeneous nonstoichiometric composition.

IV. DATA ANALYSIS

We propose to analyze the jump in resistivity at the PM-AFI transition in terms of the standard theory for conduction in a nondegenerate semiconductor, characterized by parabolic bands and classical statistics; the interaction between charge carriers is accounted for in the effective mass. As several sets of Raman^{45–48} and inelastic neutron scattering experiments^{49–52} have shown, the lattice vibration mode and phonon dispersion curves are not drastically altered in passing from the PM to the AFI phase or in altering the doping levels. Hence, no attempt has been made to allow for the relatively minor variations in lattice properties with Ti_2O_3 -alloy concentration or with deviations from ideal stoichiometry. It should be clear at the outset that this is a model calculation involving drastic simplifying assumptions whose applicability to V_2O_3 -based alloys is obviously marginal. A realistic calculation taking account of the sample anisotropy and of the correct band structures would be extremely complicated even if the requisite input information were available. We therefore adopt the limited objective of attempting to assess whether one can understand the various features of the PM-AFI transitions for $(\text{V}_{1-x}\text{Ti}_x)_2\text{O}_3$ vs $\text{V}_{2(1-y)}\text{O}_3$ in terms of an elementary analysis with a minimal number of parameters.

The conductivity of such a semiconductor is given by $\sigma = n_n e u_n + n_p e u_p$, where n_n, n_p are the charge-carrier densities in the conduction and valence bands, respectively, and u_n, u_p are the corresponding mobilities; e is the magnitude of the electronic charge. For intrinsic or near-intrinsic V_2O_3 alloys we set $n_n \cong n_p \cong n$; for extrinsic V_2O_3 alloys we set $n_n = 0$. In either situation the following expression for electrical conductivity applies:

$$\begin{aligned} \sigma_I &= 2(2\pi\bar{m}kT/h^2)^{3/2} e u_p (1 + u_n/u_p) \exp(-\epsilon_\sigma/kT) \\ &\cong N_a e u_p (1 + u_n/u_p) \exp(-\epsilon_\sigma/kT), \end{aligned} \quad (1)$$

in which ϵ_σ is the conductivity activation energy and \bar{m} is an effective mass discussed below; all other symbols retain their conventional significance. For near intrinsic materials $\bar{m} \equiv (m_n m_p)^{1/2}$ is the geometric mean of the effective charge-carrier masses, and $\epsilon_\sigma = \epsilon_g/2$, where ϵ_g is the energy gap. For essentially extrinsic materials, $\bar{m} \equiv m_p$, $u_n/u_p = 0$, and $\epsilon_\sigma \equiv \epsilon_a/2$, where ϵ_a is the energy of acceptor levels relative to the band edge associated with the presence of Ti or of vanadium vacancies. In the intervening stages Eq. (1) is still expected to provide a formal in-

terpretation of the experimental data, with

$$u_n + u_p \equiv u_p (1 + u_n/u_n) \geq u_p$$

and with $\epsilon_\sigma = \epsilon_F - \epsilon_V$, where ϵ_F and ϵ_V are the Fermi level and the valence-band edge, respectively. Note the implicit assumption that all charge carriers are itinerant. We now inquire as to how well Eq. (1) copes with the conductivity data.

Let σ_M be the conductivity of $(\text{V}_{1-x}\text{Ti}_x)_2\text{O}_3$ or of $\text{V}_{2(1-y)}\text{O}_3$ in the metallic state above the transition temperature, T_N (this quantity depends only weakly on temperature). Equation (1) may be then reformulated as

$$\begin{aligned} \ln(\sigma_I/\sigma_M) &= \ln[(2/\sigma_M)(2\pi\bar{m}kT/h^2)^{3/2} \\ &\quad \times e(1 + u_n/u_p)u_p] - \epsilon_\sigma/kT. \end{aligned} \quad (2)$$

In terms of the resistivity ρ_I and ρ_M of the insulating and metallic phases close to the transition temperature, Eq. (2) may be written as

$$\log_{10}(\rho_I/\rho_M) = -\log_{10}E + \epsilon_\sigma/2.303kT, \quad (3a)$$

in which

$$\begin{aligned} E \equiv F u_p &= [(2/\sigma_M)(2\pi m_0 k/h^2)^{3/2} \\ &\quad \times e(1 + u_n/u_p)] (\bar{m}/m_0)^{3/2} T^{3/2} u_p \\ &\equiv F_0 (\bar{m}/m_0)^{3/2} T^{3/2} u_p, \end{aligned} \quad (3b)$$

where m_0 is the free-electron mass.

To complete the analysis it is necessary to specify u_p . Two scattering mechanisms should be of relevance to the present work, namely lattice vibrational (l) and ionized-impurity (i) scattering. These are added according to the well-established additivity rule for the inverse average relaxation times, namely $\tau^{-1} = \tau_l^{-1} + \tau_i^{-1}$. However, this superposition presents problems if the relaxation times exhibit a strong energy dependence. Thus, in view of the many assumptions already adopted so far, this refinement was omitted, and a simplified analysis was introduced for each system.

V. $(\text{V}_{1-x}\text{Ti}_x)_2\text{O}_3$ -ALLOY SYSTEM

In the $(\text{Ti}_{1-x}\text{V}_x)_2\text{O}_3$ -alloy system the replacement of vanadium by titanium should not greatly alter the effective charge resident at the cation centers, nor should there be severe perturbations in the environment of the substituent. For these alloys it therefore appears reasonable to introduce lattice vibrations via acoustic modes as the principal scattering model. Standard theory shows that⁵³ the mobility is given by

$$u_p = (2^{3/2}\pi^{1/2}e\hbar^4 d_0 V_l^2 / 3m^{5/2} D_1^2 k^{3/2}) T^{-3/2} \quad (4a)$$

$$\equiv C_0 (m_0/m)^{5/3} T^{-3/2}, \quad (4b)$$

in which d_0 is the density, V_l is the sound velocity, and D_1 is the deformation potential.

When Eq. (4b) is inserted in (3b) the explicit temperature dependence cancels out, and if one equates \bar{m} with m , one finds

$$E = F_0 C_0 (m_0/m). \quad (5)$$

Then, according to Eq. (3a) the difference

$$\Delta \equiv \log_{10}(\rho_I/\rho_M)_{T_N} - \epsilon_\sigma/2.303kT_N = -\log_{10}E, \quad (6)$$

computed at the various PM-AFI transition temperatures T_N , should be given by the quantity on the right. Insertion of Eqs. (5), (4b), and (3b) shows that, in the first approximation, Δ is a constant. This concept is tested in Fig. 5 which exhibits plots of $\log_{10}(\rho_I/\rho_M)$ and of $\epsilon_\sigma/2.303kT_N$ vs T_N . It is evident that the two curves do run roughly parallel, as required by Eq. (6); however, one would expect a breakdown at low temperatures where the lattice mode excitations are less in evidence, and where ionized-impurity scattering should become increasingly important. Moreover, we have neglected any variations of σ_M , u_n/u_p , d_0 , V_l , D_1 , and \bar{m} with temperature.

As a second test concerning the proposed scattering mechanism, the E values deduced from Eqs. (3b) and (4a) were compared to the experimental value determined from Eq. (6). For computational purposes the following parameters were adopted. (i) $(1+u_n/u_p)=1.5$; this ignores the fact that in the extrinsic regime this value reduces to unity. (ii) $\sigma_M=3.5 \times 10^3 (\Omega \text{ cm})^{-1}$, as read off from Fig. 1. (iii) $d_0=4.8 \text{ g/cm}^3$. (iv) $V_l=7 \times 10^5 \text{ cm/sec}$; this value was reported for undoped V_2O_3 by Nichols, Sladek, and Harrison.⁵⁴ (v) $D_1=30 \text{ eV}$; this estimate was adopted in calculations⁵⁵ pertaining to VO_2 . (vi) T_N and ϵ_σ were read off from the data on which Fig. 5 is based.

On this basis one can determine the quantity $\log_{10}E_0 \equiv \log_{10}F_0C_0 = -1.7$ via Eqs. (5), (4), and (3). To match up with the Δ values as calculated according to Eq. (6) it is necessary to restrict the effective-mass ratio in Eq. (5) to the range $0.025 < \bar{m}/m_0 < 0.25$. The limits are set by the fact that the two curves in Fig. 5 are not exactly parallel, so that Δ in Eq. (6) covers a range from 2.65 at 125 K to 1.05 at 29 K. In view of the uncertainty in the values of the parameters listed earlier, and considering the many assumptions inherent in the comparison process, the adoption of the lattice scattering model in interpreting the

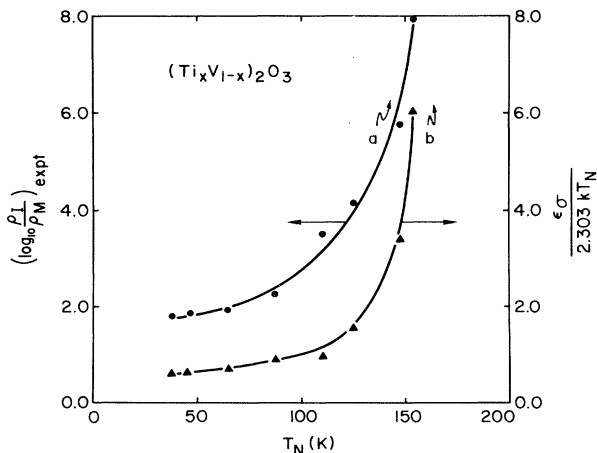


FIG. 5. Plots of $\log_{10}(\rho_I/\rho_M)$, curve a , and of $\epsilon_\sigma/2.303kT_N$, curve b , vs T_N as a test of Eq. (6) for acoustic lattice mode scattering in $(\text{V}_{1-x}\text{Ti}_x)_2\text{O}_3$.

PM-AFI transition in $(\text{V}_{1-x}\text{Ti}_x)_2\text{O}_3$ seems justified; however, the effective-mass ratios computed on this basis are rather smaller than one would have anticipated. These ratios may be increased simply by assuming a larger value for the product $d_0V_l^2/D_1^2$. With the indicated uncertainties in V_l and D_1 , it is easy to alter these parameters in a manner so as to increase both limits on \bar{m}/m_0 by 1 order of magnitude.

The above is thus consistent with the view that acoustic vibrations dominate the charge-carrier scattering process in the AFI phase of $(\text{V}_{1-x}\text{Ti}_x)_2\text{O}_3$ at temperatures close to $T=T_N$. The steady decrease in the resistivity discontinuity $\log_{10}\rho_I - \log_{10}\rho_M$ of Fig. 1 must then be attributed primarily to the observed diminution of $\epsilon_\sigma/2.303kT_N$ with T_N as documented by curve b of Fig. 5.

VI. NONSTOICHIOMETRIC V_2O_3

The conduction properties of nonstoichiometric V_2O_3 may be handled again via Eq. (3a). However, examination of Fig. 6 shows that the experimental plots of $\log_{10}(\rho_I/\rho_M)$ (curve a) and of $\epsilon_\sigma/2.303kT_N$ (curve c) vs T_N are no longer parallel, as would be demanded by Eq. (6) if E were constant. Rather, curve a of Fig. 6 passes through a minimum and then rises again with increasing departures from stoichiometry, whereas curve c drops off monotonically with T_N . One can reconcile these features by invoking ionized-impurity scattering as the model that governs the mobility. Such a step seems appropriate since incorporation of excess oxygen into V_2O_3 is accompanied by generation of cation vacancies, each of which is associated with a trivalent negative charge that serves as a scattering center.

The specification of u_p proceeds according to the theory of Dingle⁵⁶ who derived the following expression for non-degenerate semiconductors:

$$u_p = AT^3/N_i Zg(\xi), \quad (7a)$$

where in the cgs system of units,

$$A \equiv 8\sqrt{2}\kappa^2 k^{3/2}/e^3 \bar{m}^{1/2} \pi^{3/2} \equiv A_0(m_0/\bar{m})^{1/2}, \quad (7b)$$

$$g(\xi) \equiv \ln(1+\xi) - \xi/(1+\xi), \quad (7c)$$

$$\xi \equiv (8\pi\kappa mT/e^2 h^2 n)\epsilon^{3/2}. \quad (7d)$$

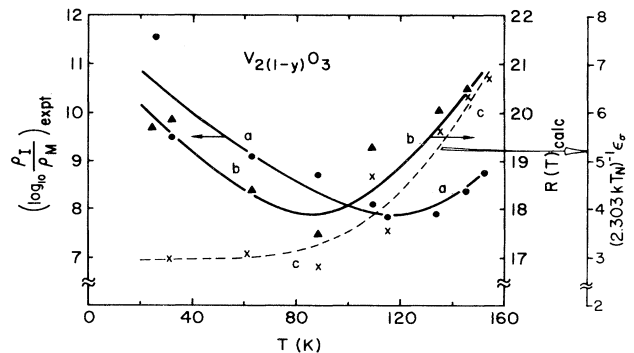


FIG. 6. Plots of $\log_{10}(\rho_I/\rho_M)$, curve a , of $R(T_N)$ via Eq. (9), curve b , and of $\epsilon_\sigma/2.303kT_N$, curve c , vs T_N , as a test of Eq. (8) for ionized-impurity scattering in $\text{V}_{2(1-y)}\text{O}_3$.

Aside from the definitions already introduced earlier, Ze is the charge on each scattering center, κ is the background dielectric constant, ϵ represents the energy of the itinerant charge carrier in the band, which is usually equated with $3kT$, and n is the charge-carrier density given by the factors $N_a \exp(-\epsilon_\sigma/kT)$ of Eq. (1). Note that N_i , the density of ionized-impurity centers, is related to N_v , the density of lattice vacancies, via⁵⁷

$$N_i = \sqrt{2N_a N_v} \exp(-\epsilon_a/2kT). \quad (7e)$$

Upon substituting Eq. (7) into Eq. (3) one obtains

$$\begin{aligned} \log_{10}(\rho_I/\rho_M)_{T_N} = & -\log_{10}(A_0 F_0 \bar{m}/m_0 Z^2) + \log_{10}g(\zeta) \\ & + \log_{10}N_v - 3 \log_{10}T_N + \log_{10}(\rho_M^0/\rho_M) \\ & + \epsilon_\sigma/2.303kT_N. \end{aligned} \quad (8)$$

Here F_0 is the factor already used in Eq. (3b), the term $\log_{10}(\rho_M^0/\rho_M)$ corrects for the difference in metallic resistivities at $T=T_N$ of the nonstoichiometric V_2O_3 (ρ_M), as opposed to the Ti-doped V_2O_3 (ρ_M^0) samples, and the rest of the terms arise from the use of Eq. (7). It should be noted that for the $(V_{1-x}Ti_x)_2O_3$ -alloy system the $\log_{10}N_i$, $\log_{10}g(\zeta)$, and $3 \log_{10}T_N$ terms are absent from Eq. (3); it is this feature which distinguishes the present analysis from that of the last section.

To test the applicability of Eq. (8), the quantity $R(T_N)$, given by

$$\begin{aligned} R(T_N) \equiv & \log_{10}g(\zeta) + \log_{10}N_i - 3 \log_{10}T_N \\ & + \log_{10}(\rho_M^0/\rho_M) + \epsilon_\sigma/2.303kT_N, \end{aligned} \quad (9)$$

was calculated for various T_N and plotted as curve *b* in Fig. 6. For the calculations the following parameters were adopted. (i) $\kappa=24$ as the low-frequency dielectric constant. No measurements of κ for the AFI phase of V_2O_3 have been published; the particular choice adopted here will be discussed further below. (ii) N_i values for use in Eq. (7c) were determined from the annealing treatment of each sample, using the information of Ref. 41. (iii) $Z=1$, based on the assumption that only one of three carriers localized on each lattice vacancy at $T=0$ is ionized at $T=T_N$. One should also note that any additional screening of the vacancy by mobile charge carriers in its immediate vicinity is simulated by the function $g(\zeta)$. (iv) ρ_M^0 was furnished in the preceding section, and ρ_M read off from Fig. 2. (v) The value $\bar{m}/m_0=1$ was adopted; this choice will be discussed further below. (vi) T_N and ϵ_σ were read off from the data on which Fig. 6 is based.

Comparison of curves *b* and *a* in Fig. 6 shows that the actual variation of $\log_{10}(\rho_I/\rho_M)$ with T_N is reasonably well reproduced by Eq. (9), although the considerable scatter in both the theoretical and experimental points precludes a detailed comparison. At the high end of the T_N range $R(T_N)$ rises more gradually than does the experimentally observed values of $\log_{10}(\rho_I/\rho_M)$. This discrepancy probably arises because lattice scattering should begin to contribute significantly to ρ_I ; no allowance has been made for this effect. The faster rise in $\log_{10}(\rho_I/\rho_M)$ with increasing T_N at the high-temperature end may be simulated by allowing κ to increase slowly in

this range. That κ should in fact be variable is plausible from Ziman's discussion,⁵⁸ where he showed that $\kappa=1+\omega_p^2/\epsilon_g^2$, where ω_p is the plasma frequency and ϵ_g the gap. Even a small decrease in ϵ_g , such as might readily be caused by changes in sample stoichiometry, would suffice to eliminate the discrepancy between curves *a* and *b* at higher T_N values. However, it was not deemed worthwhile to proceed with this refinement because the necessary information is lacking and because the entire analysis leading to Eq. (9) is based on an oversimplified model. The principal objective was to demonstrate that use of a very elementary theory invoking ionized-impurity scattering leads to far better agreement with experiment than does the theory of lattice vibration scattering, in coping with the variation of $\log_{10}(\rho_I/\rho_M)$ vs T_N for the $V_{2(1-y)}O_3$ system.

A second test involves a comparison of the calculated magnitude of the first term in Eq. (8) with the difference between curves *b* and *c* in Fig. 6. For this purpose A_0 was determined from Eq. (7b) with $\kappa=24$ and F_0 was determined from Eq. (3b) with σ_M read off from Fig. 2 using $u_n/u_p=0.5$ as a reasonable average value. To force agreement with experiment one must impose the limits $0.0075 < \bar{m}/m_0 < 2$ on the effective-mass ratio; the large range results from the fact that curves *a* and *b* of Fig. 6 do not run precisely parallel, so that the exact value of \bar{m}/m_0 depends on what portions of the two curves are forced into coincidence. One must bear in mind that the value $\bar{m}/m_0=1$ was arbitrarily selected in the calculation of $g(\zeta)$, which is consistent with the above limits. A separate calculation has indicated that if \bar{m}/m_0 is decreased by 1 order of magnitude then the function $R(T)$ no longer properly tracks the upswing of $\log_{10}(\rho_I/\rho_M)$ at low T_N values; this fact requires the effective mass be close to the free-electron mass. The reduction of the dielectric constant to a value $\kappa=2.4$ was found to shift both of the limits on m/m_0 upward by one order of magnitude, but not to alter any other features. Overall, it is seen that the ionized-impurity scattering model properly mimics the observed experimental features in $V_{2(1-y)}O_3$.

VII. CONCLUSION

A case has been made for interpreting the PM-AFI transitions in Ti-doped or in nonstoichiometric V_2O_3 through the physical properties of an itinerant standard semiconductor subject to classical statistics. Implicit in the discussion is the fundamental assumption that the use of Ti as a dopant or the generation of V vacancies introduces acceptor centers, so that on increasing their concentrations the V_2O_3 host material gradually becomes more extrinsic. This causes the Fermi level to move progressively closer to the valence-band edge, thereby reducing the number (or conductivity) activation energy ϵ_σ as the acceptor center concentration is increased.

On this basis it is possible to understand, on a nearly quantitative basis, the difference in the PM-AFI transitions for $(V_{1-x}Ti_x)_2O_3$ as compared to $V_{2(1-y)}O_3$. It is postulated that lattice scattering predominates at temperatures slightly below the transition point T_N for the Ti-doped system, in which case the resistivity jump is dom-

inated by the value of ϵ_g/kT_N ; since the latter ratio diminishes with T_N , the discontinuities become progressively smaller in Fig. 1. On the other hand, for nonstoichiometric V_2O_3 , ionized-impurity scattering is assumed to dominate. Now the effect of lowering ϵ_g/kT_N is counteracted by the increase in concentration of scattering centers; both of these features are further modified by changes in screening and by the explicit temperature dependence in Eq. (8). These various factors account for the mild dip and subsequent rise in discontinuity of the resistivity curves displayed in Fig. 2. While the theoretical development provided in preceding section is undoubtedly oversimplified the principal features of the experimental results are reasonably well reproduced with a set of parameters that are tenuous acceptable. Some improvement in experimental fit can be achieved by allowing the appropriate experimental parameters to vary with doping: As the Ti content is increased the sound velocity and de-

formation potentials undoubtedly change to some extent; similarly, the dielectric constant is altered with the cation-vacancy concentration. However, these avenues have not been pursued because of lack of the requisite information, and because the basic models are too crude to warrant such refinements.

ACKNOWLEDGMENTS

The authors are very grateful to Professor J. Appel (University of Hamburg) for a series of stimulating discussions concerning the analysis of the data. They are indebted to H. R. Harrison and C. J. Sandberg for assistance in crystal growth, and to B. F. Griffing, J. P. Shepherd, and R. Aragón for technical assistance in the measurements. This research was supported on National Science Foundation—Materials Research Laboratories program Grant No. DMR-80-20249.

*Present address: IBM Thomas J. Watson Research Center, Yorktown Heights, NY 10598.

- ¹D. B. McWhan, J. P. Remeika, T. M. Rice, W. F. Brinkman, J. P. Maita, and A. Menth, *Phys. Rev. Lett.* **27**, 941 (1971).
- ²V. A. Perelyaev and G. P. Shveikin, *Izv. Akad. Nauk. SSSR Neorg. Mater.* **7**, 892 (1971).
- ³F. Maillot and R. A. Pâris, *C. R. Acad. Sci. C* **277**, 207 (1973).
- ⁴D. B. McWhan, A. Menth, J. P. Remeika, W. F. Brinkman, and T. M. Rice, *Phys. Rev. B* **7**, 1920 (1973).
- ⁵V. A. Perelyaev, G. P. Shveikin, and G. V. Bazuev, *Tr. Inst. Khim. Ural. Nauch. Tsentr. Akad. Nauk SSSR* **25**, 8 (1971).
- ⁶V. A. Perelyaev and G. P. Shveikin, *Tr. Inst. Khim. Ural. Nauch. Tsentr. Akad. Nauk SSSR* **25**, 13 (1973).
- ⁷G. V. Chandrashekar, S. H. Shin, A. Jayaraman, J. E. Keem, and J. M. Honig, *Phys. Status Solidi A* **29**, 323 (1975).
- ⁸J. E. Keem and J. M. Honig, *Phys. Status Solidi A* **28**, 335 (1975).
- ⁹A. V. Motornyi, B. A. Tallychik, S. P. Teslenko, and B. A. Shustrov, *Fiz. Tverd. Tela (Leningrad)* **17**, 324 (1975) [*Sov. Phys.—Solid State* **17**, 198 (1975)].
- ¹⁰H. Kuwamoto, H. V. Keer, J. E. Keem, S. A. Shivashankar, L. L. Van Zandt, and J. M. Honig, *J. Phys. (Paris) Colloq.* **37**, C4-35 (1976).
- ¹¹B. A. Tallychik, B. A. Shustrov, V. N. Novikov, and E. I. Gindin, *Fiz. Tverd. Tela (Leningrad)* **18**, 1461 (1976) [*Sov. Phys.—Solid State* **18**, 868 (1976)].
- ¹²B. Brach, I. E. Grey, and C. Li, *J. Solid State Chem.* **20**, 29 (1977).
- ¹³C. E. Rice and W. R. Robinson, *J. Solid State Chem.* **21**, 145 (1977).
- ¹⁴J. Dumas and C. Schlenker, *J. Magn. Magn. Mater.* **7**, 252 (1978).
- ¹⁵J. Dumas, C. Schlenker, G. Chouteau, M. Nasr-Eddine, and F. Sayetat, *J. Appl. Phys.* **49**, 1622 (1978).
- ¹⁶J. Dumas and C. Schlenker, *J. Phys. C* **12**, 2381 (1979).
- ¹⁷Y. Ueda, K. Kosuge, S. Kachi, and T. Takada, *J. Phys. (Paris) Colloq.* **40**, C2-275 (1979).
- ¹⁸J. Dumas, *Phys. Rev. B* **22**, 5085 (1980).
- ¹⁹T. Katsura and M. Hasegawa, *Bull. Chem. Soc. Jpn.* **40**, 501 (1967).
- ²⁰M. Nakahira, S. Horiuchi, and H. Ooshima, *J. Appl. Phys.* **41**, 836 (1970).
- ²¹V. N. Novikov, B. A. Tallychik, E. I. Gindin, and V. G. Prokhorov, *Fiz. Tverd. Tela (Leningrad)* **12**, 2565 (1970) [*Sov. Phys.—Solid State* **12**, 2061 (1971)].
- ²²D. B. McWhan, A. Menth, and J. P. Remeika, *J. Phys. (Paris) Colloq.* **32**, C1-1079 (1971).
- ²³M. S. Kozyreva, V. N. Novikov, and B. A. Tallychik, *Fiz. Tverd. Tela (Leningrad)* **14**, 749 (1972) [*Sov. Phys.—Solid State* **14**, 639 (1972)].
- ²⁴V. G. Zubkov, I. I. Matveenko, B. A. Tallychik, and P. V. Gel'd, *Fiz. Tverd. Tela (Leningrad)* **13**, 3532 (1971) [*Sov. Phys.—Solid State* **13**, 2885 (1972)].
- ²⁵K. Nagasawa, Y. Bando, and T. Takada, *J. Cryst. Growth* **17**, 143 (1972).
- ²⁶N. Kimizuka, M. Ishii, M. Saeki, M. Nakano, and M. Nakahira, *Solid State Commun.* **12**, 43 (1973).
- ²⁷D. B. McWhan, J. P. Remeika, J. P. Maita, H. Okinaka, K. Kosuge, and S. Kachi, *Phys. Rev. B* **7**, 326 (1973).
- ²⁸M. Noguichi, N. Kimizuka, T. Chiba, and N. Tsuda, *J. Phys. Soc. Jpn.* **34**, 661 (1973).
- ²⁹H. Ooshima, *Yogyo Kyokai Shi* **81**, 162 (1973).
- ³⁰M. Pouchard and J.-C. Launay, *Mater. Res. Bull.* **8**, 95 (1973).
- ³¹S. Shirasaki and H. Ooshima, *Muki Zaishitsu Kenkyusho Kenky Hokohusho* **11**, 52 (1973).
- ³²J. A. Vasil'eva and I. S. Sukhushina, *J. Chem. Thermodyn.* **7**, 5 (1975).
- ³³J.-C. Launay, M. Pouchard, and R. Ayroles, *J. Cryst. Growth* **36**, 297 (1976).
- ³⁴Y. Ueda, K. Kosuge, S. Kachi, T. Shinjo, and T. Takada, *Mater. Res. Bull.* **12**, 87 (1977).
- ³⁵Y. Ueda, K. Kosuge, S. Kachi, H. Yasuoka, N. Nishihara, and H. Heidemann, *J. Phys. Chem. Solids* **39**, 1281 (1978).
- ³⁶H. Kuwamoto and J. M. Honig, *J. Solid State Chem.* **32**, 335 (1980).
- ³⁷(a) Y. Ueda, K. Kosuge, and S. Kachi, *J. Solid State Chem.* **31**, 171 (1980); (b) D. Adler, J. Feinleib, H. Brooks, and W. Paul, *Phys. Rev.* **155**, 851 (1967).
- ³⁸J. C. C. Fan and T. B. Reed, *Mater. Res. Bull.* **7**, 1403 (1972).
- ³⁹J. E. Keem, H. R. Harrison, S. P. Faile, H. Sato, and J. M. Honig, *Am. Ceram. Soc. Bull.* **56**, 1022 (1977).
- ⁴⁰H. R. Harrison, R. Aragón, and C. J. Sandberg, *Mater. Res.*

- Bull. 15, 571 (1980).
- ⁴¹S. A. Shivashankar, R. Aragón, H. R. Harrison, C. J. Sandberg, and J. M. Honig, *J. Electrochem. Soc.* 128, 2472 (1981); *ibid.* 129, 1641(E) (1982).
- ⁴²B. Griffing and S. A. Shivashankar, *Rev. Sci. Instrum.* 48, 1225 (1977).
- ⁴³A. P. B. Sinha, G. V. Chandrashekhar, and J. M. Honig, *J. Solid State Chem.* 12, 402 (1975).
- ⁴⁴N. Otsuka, H. Sato, G. L. Liedl, and J. M. Honig, *J. Solid State Chem.* 44, 230 (1982).
- ⁴⁵N. Kuroda and H. Y. Fan, *Phys. Rev. B* 16, 5003 (1977).
- ⁴⁶D. N. Mirlin and I. I. Reshina, *Fiz. Tverd. Tela (Leningrad)* 19, 201 (1977).
- ⁴⁷C. Tatsuyama and H. Y. Fan, *Phys. Rev. B* 21, 2977 (1980).
- ⁴⁸A. Okamoto, Y. Fujita, and C. Tatsuyama, *J. Phys. Soc. Jpn.* 52, 312 (1983).
- ⁴⁹R. E. Word, S. A. Werner, W. B. Yelon, J. M. Honig, and S. A. Shivashankar, *Phys. Rev. B* 23, 3533 (1981).
- ⁵⁰W. B. Yelon, S. A. Werner, R. E. Word, J. M. Honig, and S. A. Shivashankar, *J. Appl. Phys.* 52, 2237 (1981).
- ⁵¹W. B. Yelon, S. A. Werner, S. A. Shivashankar, and J. M. Honig, *Phys. Rev. B* 24, 1818 (1981).
- ⁵²M. Yethiraj, S. A. Werner, W. B. Yelon, and J. M. Honig, in *Neutron Scattering—1981 (Argonne National Laboratory)*, edited by J. Faber, Jr. (AIP, New York, 1982), p. 343.
- ⁵³R. S. Smith, *Semiconductors* 2nd ed. (Cambridge University Press, London, 1978), Chap. 8.
- ⁵⁴D. N. Nichols, R. J. Sladek, and H. R. Harrison, *Phys. Rev. B* 24, 3025 (1981); D. N. Nichols and R. J. Sladek, *ibid.* 24, 3155 (1981).
- ⁵⁵M. Gupta, A. J. Freeman, and D. E. Ellis, *Phys. Rev. B* 16, 3338 (1977).
- ⁵⁶R. B. Dingle, *Philos. Mag.* 40, 831 (1955).
- ⁵⁷J. S. Blakemore, *Solid State Physics* (Saunders, Philadelphia, 1969), Sec. 4.1.
- ⁵⁸J. M. Ziman, *Principles of the Theory of Solids*, 2nd ed. (Cambridge University Press, New York, 1972), Sec. 5.6.